Asymmetric ionic aerogel of biologic nanofibrils for harvesting electricity from moisture

Yang, Weiqing; Li, Xiankai; Han, Xiao; Zhang, Weihua; Wang, Zengbin; Ma, Xiaomei; Li, Mingjie; Li, Chaoxu

Published in:
Nano Energy

DOI:
10.1016/j.nanoen.2020.104610

Published: 14/02/2020

Document Version
Final published version

Asymmetric Ionic Aerogel of Biologic Nanofibrils for Harvesting Electricity from Moisture

Weiqing Yang,[a] *Xiankai Li,*[b,c] *Xiao Han,*[b,c] *Weihua Zhang,*[d] *Zengbin Wang,*[b] *Xiaomei Ma,**[a] *Mingjie Li**[b,c] *and Chaoxu Li,**[b,c]

[a]College of Chemistry and Chemical Engineering, Qingdao University, 308 Ningxia Road, Qingdao, Shandong 266071, P. R. China

[b]Group of Biomimetic Smart Materials, Qingdao Institute of Bioenergy and Bioprocess Technology, Chinese Academy of Sciences, Songling Road 189, Qingdao 266101, P. R. China

[c]Center of Material and Optoelectronics Engineering, University of Chinese Academy of Sciences, 19A Yuquan Road, Beijing 100049, P. R. China

[d]Johan Gadolin Process Chemistry Centre, c/o Laboratory of Wood and Paper Chemistry, Åbo Akademi University, Turku FI-20500, Finland

*Corresponding authors: Xiaomei M (mxm@qdu.edu.cn), Mingjie Li (limj@qibebt.ac.cn) and Chaoxu Li (licx@qibebt.ac.cn)

Abstract

Artificial asymmetric ionic membranes have attracted great interests in harvesting electricity from ubiquitous water activities, while mostly based on delicately-designed nanopores/nanochannels, either to harness saline water in mimic of cytomembranes or to harness moisture with carbon nanomaterials. Herein, fully biological asymmetric ionic aerogels were fabricated from biological oppositely-charged nanofibrils through a facile freeze-casting method. When exposing to moisture, these nanofibrils may be hydrated by capturing moisture and thus simulate the charged nanochannels for ion transport. Ion dissociation and diffusion ions would induce directional movement of charges, thereby leading to a potential up to 115 mV. With sustainability, biocompatibility and biodegradability, these biological nanogenerators may promise a low-cost and high-efficiency electricity harvest strategy from moist air, being capable of serving as self-powered wearable, biomedical and miniaturized electronic devices.

Keywords*:* Asymmetric ionic aerogel; Biological nanofibrils; Electricity harvest; Moisture.

1. Introduction

Porous Janus membranes, i.e., porous membranes with asymmetric properties (e.g., chemical compositions, wettability, charges and porosity) on each side, have shown great potential in various energy-efficient applications (e.g., emulsification [1], demulsification [2], fog harvesting [3] and energy harvesting [4]), because of their super capabilities of reducing permeating resistance of specific gases and liquids, and further allowing their selective mass transport. In particular, asymmetric surface charges of porous membranes, which enable selective permeation of anions or cations in mimic of cell membranes [5, 6], have been implemented in electrodialysis [7], ionic rectification [8], and nanofiltration of charged nanomaterials [9], *etc* [10, 11]. Besides these, asymmetric ionic membranes have also shown great superiority in harvesting electricity from ubiquitous waters (e.g., salinity gradient [12] and moisture [13]) for applications in flexible, wearable and biomedical devices. However, in most cases these asymmetric ionic membranes were based on the delicately-designed nanopores/nanochannels (e.g., made of anodic aluminum oxide (AAO) [12, 14], block copolymers [4], closely packing particles [15] and graphene [13]). Owing to uncontrollable and broad-range nanopores sizes, biological fibrous membranes, despite having broad applications in filtration/separation membranes [16, 17], have rarely been endeavored to serve as asymmetric ionic membranes, especially for the purpose of harvesting energy for water activities (e.g., evaporation, diffusion and flow).

Within a charged nanopore/nanochannel with its radius comparable to the Debye length of the ionic solution, its surface charges would produce an electric double layer, and then influence both the enrichment and transport of anions and cations [18]. In order to avoid the possible presence of ionic concentration polarization for selective and efficient ion transport, asymmetric ionic channels were normally introduced to optimize the ion-enrichment and ion-depletion effects [19]. For example,

anion/cation diode-like selective transport was achieved by asymmetric ionic nanochannel membranes of polyimide [20], polyamide [21], polyethylene terephthalate (PET) [22] and closely packing silica nanoparticles [15]. Ionic rectification with the ratio up to hundreds was obtained with asymmetric conical PET nanochannel with opposite surface charge [23]. Electricity was also harvested from salinity gradient and osmotic energy of saline water, based on asymmetric ionic channels of AAO [12, 14], block copolymers [4], and mesoporous carbon [12].

Besides harvesting energy from saline water, asymmetric ionic membranes could also be employed to harvest electricity from moisture. In contrast to saline water, moisture from industry, natural evaporation and physiological processes (e.g., transpiration and respiration) is more ubiquitous and spontaneous in the environment, and thus capable of affording a huger application potential for facile and low-cost electricity generation. In most cases, the asymmetric ionic membranes were produced from carbon nanomaterials (e.g., graphene oxides) with a gradient distribution of charged groups (e.g., carboxyl) [13, 24-27]. When exposing to moisture, adsorption and condensation of moisture occurred within the inner pores of nanomaterials [13, 24, 25, 28-30]. Ions (e.g., H^+ and H_3O^+) may be dissociated with a concentration gradient, and thus generate a transmembrane electric pulse [13, 25, 26, 29, 30]. Notably, electric potential arising from waterflow would also be possible during this process, according to the mechanisms of stream potential [31, 32], electron drag [33], ion hopping [34], polarization-induced-dissociation effect [35], and charge exchange between water molecules and carbon nanomaterials [36].

In order to relieve environmental/cytotoxic concerns for wide use of high-cost inorganic/carbon nanomaterials [28, 37, 38], sustainable biomaterials have attracted great interests in harvesting energy from water activities [39]. In particular, we found that biological nanofibrils (NFs) with charged

surfaces may be hydrated in moisture and serve equivalently as the charged nanochannels for energy harvest from moist air flow [40]. With comparison to inorganic nanomaterials and synthetic polymers [41, 42], biologic nanomaterials have the advantages of abundant functional groups and facileness of chemical modification. Thus, in this study asymmetric ionic aerogel was produced from 2,2,6,6-tetramethylpiperidine-1-oxyl-oxidized cellulosic NFs (i.e., TEMPO-CNFs) and quaternized cellulosic NFs (i.e., Quatern-CNFs) in a facile directional-freeze casting method. When exposed to moist air, the asymmetric ionic aerogel could induce an open circuit potential (V_{oc}) as high as ~115 mV with a maximum short circuit current (I_{sc}) of 45 nA, which is a comparable or superior overall performance compared with reported moisture-driven generators (see details in Table S1). This production strategy also maintained valid for other types of biological nanofibrils with oppositely charged states, such as amyloid fibrils of bovine serum albumin (BSA)/chitin NFs, carboxylated silk NFs/chitin NFs, BSA NFs/lysozyme NFs, TEMPO-CNFs/chitin NFs and TEMPO-CNFs/lysozyme NFs.

With comparison to the asymmetric ionic nanopores/channels reported in the literature, biological nanofibrils were not only sustainable and low-cost, but also promising to avoid complicated procedures for nanochannel production and surface treatment (e.g., plasma, laser and harsh oxidation). Their facile procedures of surface chemical modification also ensured to produce asymmetric membranes with opposite charges on each side, in contrast to gradient distributions of charges groups in asymmetric ionic membranes of graphene oxides [13]. Thus, in addition to harvesting electricity from moist air flow by using mono-component aerogels of biological nanofibrils [40], electricity could also be harvested directly from more ubiquitous moist air through this bilayer type of asymmetric ionic aerogel, which may promise a low-cost and high-efficiency handy power supply solution, and facilitate wide applications of innovative self-powered electronic devices.

2. Experimental section

2.1 Fabrication of asymmetric ionic aerogel

Fabrication of silk NFs, amyloid NFs, deacetylated chitin NFs and BSA NFs was detailed in Supporting Information. Aerogels were fabricated with the suspensions of these NFs. Typically, a suspension of Quatern-CNFs (0.3–0.6 wt%) was poured into a mold, followed by subjecting to unidirectional freezing with liquid nitrogen. Unidirectional freezing was also performed after pouring another solution of Tempo-CNFs (0.3–0.6 wt%). The asymmetric bilayer aerogel (2–10 mm in thickness) was obtained by freeze-drying in a freeze drier (FD-1C-50, Beijing BoYiKang) at −55 °C. The aerogel was laminated between two electrodes of Pt nets (purchased from Global Jinxin International Technology Co., LTD , with the mesh size of 0.25 mm and diameter of Pt wires of 0.1 mm) with the size = 3 × 3, 4 × 4 or 5 × 5 cm^2, serving as the current collectors (see details in Fig. S5). The RH value was adjusted by saturated salt solutions within the enclosed environment at 25 °C, such as RH=99% (Na_2HPO_4), RH=90% (Na_2CO_3), RH=80% (NH_4Cl), RH=70% ($CO(NH_2)_2$), RH=60% (NaBr) and RH=50% ($Ca(NO_3)_2$).

2.2 Sensing measurements

The sensors were constructed by laminating the bilayer aerogel (diameter of 2 cm, thickness of 6 mm and ratio of bilayer thickness of ~1) within the Pt electrodes. For finger sensing, the sensor was fixed on a glass slide. And an index finger slowly approached to the sensor at ambient RH. Both the electric potential (V_{oc}) and the distance between the sensor and finger were measured simultaneously. For breath sensing, the sensor was integrated to a commercial aspirator (3M N95), the V_{oc} variation was recorded under strenuous exercise and relaxation states. For humidity sensing, the sensor was fixed on one hydroponic *Alocasia genus* outdoors (Qingdao in North China: East longititude ~120° and North

latitude ~36°). The V_{oc} value was recorded from 8 o'clock to 20 o'clock (Apr. 26th, 2019), together with the temperature, RH and solar density.

2.3 Characterization

Transmission electron microscopy (TEM) and field emission scanning electron microscopy (FESEM) were performed on Hitachi H-7650 (Hitachi, Japan) and JEOL 7401 (JEOL, Japan), respectively. Zeta potential was recorded on Zetasizer Nano ZSE (Malvern Instruments Ltd., England). Elemental analysis was carried out on an Elementar Analysensysteme GmbH Vario EL Cube elemental analyser. Open circuit voltage and resistance in real time were recorded using a digital multimeter (MS8265, Mastech Ltd. Dongguan, China). Short-circuit current is recorded in real time using a digital nanometer (JX-A04, Jianxin Ltd. Dongguan, China). Relative humidity values were measured by a digital RH meter (S-WS05, Shenxinhui Electronics Co., Ltd. Shenzhen, China).

3. Results and discussion

3.1 Design of asymmetric ionic nanofibrous aerogel as biological generator

Bio-macromolecules and their assemblies are characteristic of abundant functional groups and hereby opt to be chemically modified for different surface charges and charge densities [43-45]. Being one of the most fundamental building blocks of natural biomaterials, biological NFs with negative or positive surface charges could be extracted from naturally abundant biomass and/or synthesized through supramolecular self-assembly (Fig. 1a-1c & Fig. S1-S2) [40, 46]. For instance, CNFs with negative and positive charges were exfoliated mechanically from hardwood via TEMPO-mediated oxidization (i.e., TEMPO-CNFs) [47] and 2,3-epoxypropyl trimethylammonium chloride cationization (i.e., Quatern-CNFs) [48], respectively (Fig. 1a-1d); Negatively charged silk NFs (i.e., carboxylated silk NFs) were exfoliated mechanically from *Bombyx mori* cocoons through a NaClO oxidization method

(Fig. S2) [49]; And positively charged amyloid NFs were synthesized via supramolecular assembly of lysozyme at pH ~2 and 60 °C (i.e., lysozyme NFs) (Fig. S2) [50]. Negatively charged amyloid NFs were synthesized via a poor-solvent-induced fibrillation of BSA molecules (i.e., BSA NFs) (Fig. S2) [49]. All these NFs had the diameter of <10 nm and the aspect ratio of $>10^2$ (Fig. 1b & Fig. S1-S2). Among these biological NFs, charged CNFs have been studied in details, because they are one type of the most abundant biological materials in nature, and have seen diverse applications in catalysts, electro-optical films, nanofiber-reinforced composites, microelectronics, *etc* [45, 51]. Their surface charge densities and ζ-potential could be tuned precisely, e.g., 0.5~1.39 mmol g^{-1} carboxyl groups and −25~−43 mV of ζ-potential for TEMPO-CNFs, and 0.5~1.28 mmol g^{-1} quaternary ammonium groups and 30~54 mV of ζ-potential for Quatern-CNFs (Fig. S1).

Owing to their highly charged surfaces, these CNFs (~3.5 mg mL^{-1}) maintained colloidally stable at the nematic states (inset of Fig. 1b). After directionally freezing the dispersion of TEMPO-CNFs with liquid nitrogen, another layer of Quatern-CNFs dispersion was casted onto its top. Then fibrous bi-layered aerogel with oriented structure was produced through a freeze-drying process (Fig. 1e & S3). Hierarchical porosities were further revealed with the oriented microscale pores (i.e., the channel width 1−10 μm) and nanoscale pores (i.e., the size <100 nm). The aerogel porosity varied within 99.2−99.6% by tuning the CNFs concentrations in their dispersions from 3 to 6 mg ml^{-1} (Fig. S4).

The humidity-induced nanogenerator was constructed by laminating the bilayer of cellulosic aerogel (e.g., 3/3 mm/mm thick for TEMPO-CNFs/Quatern-CNFs; 2 cm in diameter) between two parallel Pt nets as current collectors (mesh size ~0.25 mm) (Fig. 1e-1f & S5). At an environmental relative humidity (RH) of ~99%, V_{oc} increased dramatically to a maximum value as high as ~115 mV at ~20 min, and then decreased gradually to vanishment within ~30 min (Fig. 1g). With alternately

160 switching moisture between On and Off, a variational period of V_{oc} was observed. This power
161 generation ability could be cyclically repeated without severe decay (Fig. 1g & S6). In addition, an I_{sc}
162 up to 45 nA was also aroused by the moisture, following the variation route similar to that of V_{oc} (Fig.
163 S6 & S7).

164 *3.2 Suggested mechanism of the biological generator*

165 Further investigation showed that low RH (e.g., <50%) produced negligible V_{oc}, while the higher RH
166 ≥50% promoted the V_{oc} value progressively up to maximum value of ~115 mV at RH ~99% (Fig. 2a
167 & S8). These phenomena confirmed that water played a vital role in this electricity-generation process.
168 To be noted, biological NFs not only had the ultrathin diameter of <10 nm and large specific surface
169 area, but also had the contents of hydrophilic groups (e.g., hydroxy, carboxyl in TEMPO-CNFs and
170 quaternary ammonium in Quatern-CNFs) higher than those of carbon nanomaterials used for moisture-
171 induced electricity generation [13, 24, 25, 28, 29]. When exposing to moist air, these fibrous aerogels
172 could easily capture moisture and immobilize water molecules via hydrogen bonding (e.g., TEMPO-
173 CNFs–O···H–OH and Quatern-CNFs–N···H–OH). And inevitably capillary condensation occurred
174 within the nanoscale pores of the aerogel according to Kelvin's equation [52]:

175 $$\ln\frac{P}{P_0}\sim\frac{\gamma}{r} \qquad (1)$$

176 where P_0 and P are the saturation vapor pressures of water near planar surface and concave meniscus,
177 respectively; r is the curvature radius of the water surface (being negative for concave meniscus); and
178 γ is the surface tension of water. For the bilayer aerogel with the hydrophilic group concentration of
179 ~0.9 mmol g^{-1} (i.e., TEMPO-CNFs with the carboxyl content of ~0.89 mmol g^{-1} and Quatern-CNFs
180 with the quaternary ammonium group of ~0.91 mmol g^{-1}, and thickness ratio of 1), the moisture uptake
181 capacity increased dramatically with the increasing RH, and got a maximum value up to ~0.9 g g^{-1}

(Fig. 2b & S9). And thus a bilayer hydrated shell would form on the surfaces of these NFs: an inner layer with immobilized water molecules and an out layer with free water molecules (Fig. 2d). Polar groups of the CNFs could release a large amount of counter ions (e.g., H^+, Na^+ and Cl^-), and built an electric double layer (EDL) [36, 53]. Therefore, an ion conductive network would form within the hydrated surface and channels of the fibrous aerogels [54]. Correspondingly, the internal resistance sharply decreased from ~100 to 0.8 MΩ when RH increased from 55 to 99% (Fig. 2b).

Due to the bilayer structure of the aerogel, cations were mainly produced within the TEMPO-CNF aerogel layer, while anions were produced mainly within the Quatern-CNF aerogel layer. Driven by the osmotic pressure, directional movement of net charges induced the potential (i.e., V_{oc}). And the consumption of the free ions osmosis and net charge transfer led to an evanescent V_{oc} (Fig. 2c). When switched to a depressed RH (RH <10%) the released ions would go back to the surfaces of NFs, and thereby produced a recyclable V_{oc} generation under "On/Off" moisture stimuli (Fig. 1f).

3.3 Structural optimization of asymmetric ionic aerogel nanogenerator

Besides the RH value, the content of charged groups on biological NFs can also play a prominent role in the device performance. V_{oc} increased obviously with an increasing concentration of charged groups as exhibited in Fig. 3a. According to Nernst equation for a concentration difference cell [55]:

$$V \sim \frac{RT}{F}\left(\left|\ln\frac{a_2^+}{a_1^+}\right| + \left|\ln\frac{a_2^-}{a_1^-}\right|\right) \quad (2)$$

where the R, T and F represent the gas constant, temperature and Faraday's constant; a_2^+ and a_1^+ refer to the activities of cations in the Quatern-CNFs side and interface of the two sides, respectively, while a_2^- and a_1^- refer to the activities of anions in the TEMPO-CNFs side and interface of the two sides, respectively. Thus, more dissociable groups would increase the number of counter ions, and thus enhance the output voltage. However, the aerogels with excessive dissociable groups (e.g., >1 mmol

204 g^{-1}) led to a slight decrease in V_{oc} at high RH values (e.g., 99%) (Fig. 3a), due to the structural collapse
205 under hydration (Fig. S10).

206 The V_{oc} value could also be tuned by the geometric structures of the fibrous aerogels (Fig. 3b-3e).
207 A larger device area seemingly led to a higher I_{sc} value (Fig. 3c). With the constant device thickness
208 (i.e., 6 mm) and dissociable group contents (e.g., ~0.9 mmol g^{-1} for carboxyl groups in TEMPO-CNFs
209 and quaternary ammonium in Quatern-CNFs), the thickness ratio of the bilayer was optimal at ~1:1,
210 owing to the nearly equal amounts of free charges. Thus the aerogel generator could be optimized with
211 the porosity of ~99.3%, the aerogel thickness of ~6 mm, and the bilayer thickness ratio of ~1:1 (Fig.3b-
212 3e). Furthermore, these nanogenerators could also be connected in series or in parallel for high V_{oc} or
213 I_{sc} (Fig. 3f & Fig. S11).

214 *3.4 Electricity-generation performance of asymmetric ionic aerogel nanogenerator*

215 The electricity generated by this biological diode generator could be conveniently accumulated and
216 stored with the conventional solutions. As shown in Fig. 4a, commercial capacitors (e.g., capacitance
217 3.3 mF) were charged with the diode generator, being able to serve as power supply for daily
218 appliances such as lighting a red LED with a driven voltage ~1.5 V (Fig. S12 & Video S1). Since
219 moisture widely exists in nature (e.g., evaporation of waters and transpiration of plants) and in industry
220 (e.g., drying and water cooling), the biological nanogenerators enable a variety of applications. For
221 instance, the generator was capable of a self-powered electrical humidity sensor with a sensitivity as
222 high as 2.35 mV/RH% (Fig. 4b), being superior to most of the humidity sensors in the literature, such
223 as porous carbon humidity sensor (~2 mV/RH%), polymer nanowire sensor (~1.3 mV/RH%),
224 graphene oxide hydrovoltaic sensor (~0.7−1 mV/RH%), graphene oxide/poly(sodium 4-
225 styrenesulfonate) composite dielectric sensor (0.0375 mV/RH%) and polyaniline piezoresistive sensor

(0.64 mV/RH%) [24, 25, 27, 41, 56, 57]. Because of the distance-determined moisture distribution near the human skin, the generator could also detect the distance away from the skin, which may promise diverse applications like touchless control and contact warning (Fig. 4c & Fig. S13) [58].

The biological nanogenerator could also be powered by some physiological processes, e.g., transpiration and perspiration, rendering huge potentials for self-powered health monitoring devices. When integrated with a commercial respirator (like 3M N95), the generator could detect the dynamic characteristics of breathing (e.g., frequency and intensity). As shown in Fig. 4d, the frequency of the V_{oc} pulses coincided with the breath before and after strenuous exercise with a breathing frequency of 20 and 38 min^{-1}. Moreover, this biologic generator could also be installed near plants to monitor and quantify their transpiration process which releases >99% of water consumed by plants into air [59]. As shown in Fig. 4e & S14, the electrical signal of this generator above one hydroponic *Alocasia genus* was collected on daytime of Apr. 26 th, 2019 (Qingdao in North China: East longitude ~120° and North latitude ~36°), which reflected the intensity of plant transpiration in real time. Furthermore, the biological generator could be fully degraded in natural soil leachate within 25 days (Fig. S15), once again demonstrating the nanogenerator ideal for next generation wearable electronic devices.

4. Conclusion

In this study, asymmetric ionic aerogels of biological NFs enabled the electric energy harvest from moisture variation. Biological NFs were not only sustainable and low-cost, but also promising in abundant functional groups and facileness of chemical modification. Asymmetric ionic aerogels were fabricated of carboxylated and quaternized cellulosic NFs through a facile directional-freeze casting method. When exposing the asymmetric aerogels to moisture, these NFs could capture water from air and formed ion conductive networks with hydrated nanochannels. Ion dissociation and diffusion would

lead to directional movement of charges, thereby producing a potential across the aerogel. The generators of asymmetric ionic aerogels could also fabricated by other biological NFs pairs such as BSA NFs/deacetylated chitin NFs, carboxylated silk NFs/deacetylated chitin NFs, BSA NFs/lysozyme NFs, TEMPO-CNFs/deacetylated chitin NFs and TEMPO-CNFs/lysozyme NFs (Fig. S16). Combining sustainability, biocompatibility and biodegradability, these biological nanogenerators may promise a low-cost and high-efficiency handy power supply strategy, as well capable of serving as self-powered wearable, biomedical and miniature electronic devices.

Acknowledgements

National Natural Science Foundation of China (No. 21474125 and 51608509), Chinese "1000 Youth Talent Program", Shandong "Taishan Youth Scholar Program", Shandong Provincial Natural Science Foundation (No. JQ201609), "135" Projects Fund of CAS QIBEBT Director Innovation Foundation and Shandong Collaborative Innovation Centre for Marine Biomass Fibre Materials and Textiles are kindly acknowledged for financial support.

References

[1] Z. Wang, Y. Wang, G. Liu, Angew. Chem. Int. Ed., 55 (2016) 1291−1294.
[2] Z. Wang, M. Lehtinen, G. Liu, Angew. Chem. Int. Ed., 56 (2017) 12892−12897.
[3] P. Zhang, B. Peng, J. Wang, L. Jiang, Adv. Funct. Mater. , 29 (2019) 1904535.
[4] Z. Zhang, X. Sui, P. Li, G. Xie, X.-Y. Kong, K. Xiao, L. Gao, L. Wen, L. Jiang, J. Am. Chem. Soc., 139 (2017) 8905−8914.
[5] P. Jin, D. Bulkley, Y. Guo, W. Zhang, Z. Guo, W. Huynh, S. Wu, S. Meltzer, T. Cheng, L.Y. Jan, Nature, 547 (2017) 118−122.
[6] G. Eric, M. Roderick, Science, 310 (2005) 1461−1465.
[7] D.A. Vermaas, M. Saakes, K. Nijmeijer, Energy Environ. Sci., 45 (2011) 7089−7095.
[8] Z. Zhang, X.Y. Kong, K. Xiao, G. Xie, Q. Liu, Y. Tian, H. Zhang, J. Ma, L. Wen, L. Jiang, Adv. Mater., 28 (2016) 144−150.
[9] J. Liu, D. Hua, Y. Zhang, S. Japip, T.S. Chung, Adv. Mater., 30 (2018) 1705933.
[10] G. Wei, T. Ye, J. Lei, Acc Chem Res, 46 (2013) 2834−2846.
[11] A. van den Berg, H.G. Craighead, P. Yang, Chem. Soc. Rev., 39 (2010) 899−900.
[12] J. Gao, W. Guo, D. Feng, H. Wang, D. Zhao, L. Jiang, J. Am. Chem. Soc., 136 (2014) 12265−12272.

[13] F. Zhao, Y. Liang, H. Cheng, L. Jiang, L. Qu, Energy Environ. Sci., 9 (2016) 912−916.
[14] W. Xin, Z. Zhang, X. Huang, Y. Hu, T. Zhou, C. Zhu, X.-Y. Kong, L. Jiang, L. Wen, Nat. Commun., 10 (2019) 3876.
[15] E. Choi, C. Wang, G.T. Chang, J. Park, Nano Lett., 16 (2016) 2189−2197.
[16] Z. Wang, J. Xu, M. Li, C. Su, X. Wu, Y. Zhang, J. You, C. Li, ACS Appl. Mater. Interfaces, 11 (2019) 8576−8583.
[17] Y. Wang, L. Zhu, J. You, F. Chen, Z. Lu, X. Yan, C. Li, Y. Wang, L. Zhu, J. You, ACS Sustainable Chem. Eng., 5 (2017) 10673−10681.
[18] H.C. Yang, Y. Xie, J. Hou, A.K. Cheetham, V. Chen, S.B. Darling, Adv. Mater., 30 (2018) 1801495.
[19] Z. Zhang, L. Wen, L. Jiang, Chem. Soc. Rev., 47 (2018) 322−356.
[20] Q. Liu, K. Xiao, L. Wen, Y. Dong, G. Xie, Z. Zhang, Z. Bo, L. Jiang, ACS Nano, 8 (2014) 12292−12299.
[21] F. Li, Z. Zhou, Small, 14 (2018) 1702961.
[22] M. Liu, H. Zhang, K. Li, L. Heng, S. Wang, Y. Tian, L. Jiang, Adv. Funct. Mater., 25 (2015) 421−426.
[23] I. Vlassiouk, Z.S. Siwy, Nano Lett., 7 (2007) 552.
[24] K. Liu, P. Yang, S. Li, J. Li, T. Ding, G. Xue, Q. Chen, G. Feng, J. Zhou, Angew. Chem., Int. Ed., 55 (2016) 8003−8007.
[25] Z. Fei, C. Huhu, Z. Zhipan, J. Lan, Q. Liangti, Adv. Mater., 27 (2015) 4351−4357.
[26] C. Yang, Y. Huang, H. Cheng, L. Jiang, L. Qu, Adv. Mater., 31 (2019) 1805705.
[27] H. Cheng, Y. Huang, L. Qu, Q. Cheng, G. Shi, L. Jiang, Nano Energy, 45 (2018) 37−43.
[28] D. Shen, M. Xiao, G. Zou, L. Liu, W.W. Duley, Y.N. Zhou, Adv. Mater., 30 (2018) 1705925.
[29] K. Hu, R. Xiong, H. Guo, R. Ma, S. Zhang, Z.L. Wang, V.V. Tsukruk, Adv. Mater., 28 (2016) 3549−3556.
[30] T. Xu, X. Ding, C. Shao, L. Song, T. Lin, X. Gao, J. Xue, Z. Zhang, L. Qu, Small, (2018) 1704473.
[31] F.H. Van der Heyden, D.J. Bonthuis, D. Stein, C. Meyer, C. Dekker, Nano Lett., 6 (2006) 2232−2237.
[32] F.H. van der Heyden, D. Stein, C. Dekker, Phys. Rev. Lett., 95 (2005) 116104.
[33] P. Král, M. Shapiro, Phys. Rev. Lett., 86 (2001) 131−134.
[34] J. Yin, Z. Zhang, X. Li, J. Zhou, W. Guo, Nano Lett, 12 (2012) 1736−1741.
[35] S. He, Y. Zhang, L. Qiu, L. Zhang, E.H. Sargent, Adv. Mater., 30 (2018) 1707635.
[36] G. Xue, Y. Xu, T. Ding, J. Li, J. Yin, W. Fei, Y. Cao, J. Yu, L. Yuan, L. Gong, J. Chen, S. Deng, J. Zhou, W. Guo, Nature Nanotechnology, 12 (2017) 317−321.
[37] Z. Zhang, X. Li, J. Yin, Y. Xu, W. Fei, M. Xue, Q. Wang, J. Zhou, W. Guo, Nat. nanotechnol., 13 (2018) 1109−1119.
[38] Y. Xu, P. Chen, H. Peng, Chem.-Eur. J., 24 (2018) 6287−6294.
[39] X. Gao, T. Xu, C. Shao, Y. Han, B. Lu, Z. Zhang, L. Qu, Journal of Materials Chemistry A, 7 (2019) 20574−20578.
[40] M. Li, L. Zong, W. Yang, X. Li, J. You, X. Wu, Z. Li, C. Li, Adv. Funct. Mater., (2019) 1901798.
[41] X. Nie, B. Ji, N. Chen, Y. Liang, Q. Han, L. Qu, Nano Energy, 46 (2018) 297−304.
[42] T. Xu, X. Ding, Y. Huang, C. Shao, L. Song, X. Gao, Z. Zhang, L. Qu, Energy Environ. Sci., 12 (2019) 972−978.
[43] M. Krishnan, N. Mojarad, P. Kukura, V. Sandoghdar, Nature, 467 (2010) 692−695.
[44] B.E. Cohen, T.B. McAnaney, E.S. Park, Y.N. Jan, S.G. Boxer, L.Y. Jan, Science, 296 (2002)

1700−1703.
[45] S. Ling, W. Chen, Y. Fan, K. Zheng, K. Jin, H. Yu, M.J. Buehler, D.L. Kaplan, Prog. Polym. Sci., 85 (2018) 1−56.
[46] X. Wu, X. Han, L. Lv, M. Li, J. You, C. Li, J. Colloid Interface Sci., 527 (2018) 117−123.
[47] T. Saito, Y. Nishiyama, J.-L. Putaux, M. Vignon, A. Isogai, Biomacromolecules, 7 (2006) 1687−1691.
[48] A. Olszewska, P. Eronen, L.-S. Johansson, J.-M. Malho, M. Ankerfors, T. Lindstrom, J. Ruokolainen, J. Laine, M. Osterberg, Cellulose, 18 (2011) 1213−1226.
[49] K. Zheng, J. Zhong, Z. Qi, S. Ling, D.L. Kaplan, Adv. Funct. Mater., 28 (2018) 1806380.
[50] J. You, M. Li, B. Ding, X. Wu, C. Li, J. You, M. Li, B. Ding, X. Wu, C. Li, Adv. Mater., 29 (2017) 1606895.
[51] L. Zhu, L. Zong, X. Wu, M. Li, H. Wang, J. You, C. Li, ACS Nano, 12 (2018) 4462−4468.
[52] S. Siboni, Am. J. Phys., 74 (2006) 565−568.
[53] K. Uetani, H. Yano, Biomacromolecules, 12 (2010) 348−353.
[54] J. Peng, D. Cao, Z. He, J. Guo, P. Hapala, R. Ma, B. Cheng, J. Chen, W.J. Xie, X.-Z. Li, Nature, 557 (2018) 701−705.
[55] W. Di, Advanced Materials Technologies, 4 (2016) 1600145.
[56] H.-W. Yu, H.K. Kim, T. Kim, K.M. Bae, S.M. Seo, J.-M. Kim, T.J. Kang, Y.H. Kim, ACS Appl. Mater. Interfaces, 6 (2014) 8320−8326.
[57] S.J. Patil, A. Adhikari, M.S. Baghini, V.R. Rao, Sensor Actuat. B: Chem, 203 (2014) 165−173.
[58] J. Feng, L. Peng, C. Wu, X. Sun, S. Hu, C. Lin, J. Dai, J. Yang, Y. Xie, Adv. Mater., 24 (2012) 1969−1974.
[59] J.M. Baker, C.H.M.V. Bavel, Plant Cell Environ., 10 (2010) 777−782.

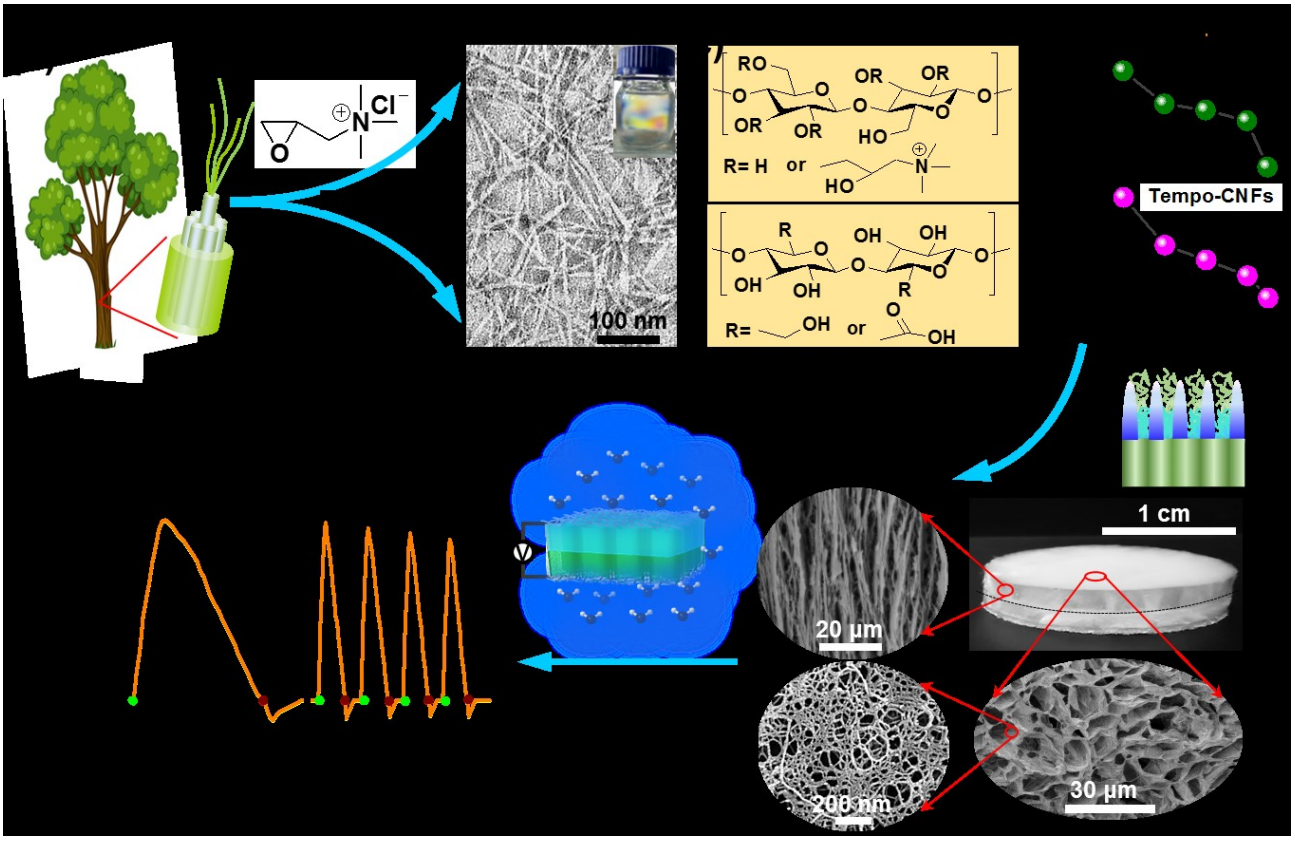

Fig. 1. Synthesis pathway of asymmetric ionic nanofibrous aerogel as biological generator. (a) Schematic illustration of synthesizing oppositely charged CNFs from wood via mechanical exfoliation. (b) Typical TEM image of negatively charged TEMPO-CNFs. (c-d) Chemical structures (c) and Zeta potentials (d) of Quatern-CNFs (top) and TEMPO-CNFs (bottom). (e) Optical and SEM images of asymmetric ionic aerogel fabricated by directional freezing and freeze drying. (f) V_{oc} generated with asymmetric ionic generator under periodic moist stimuli. RH = 99%.

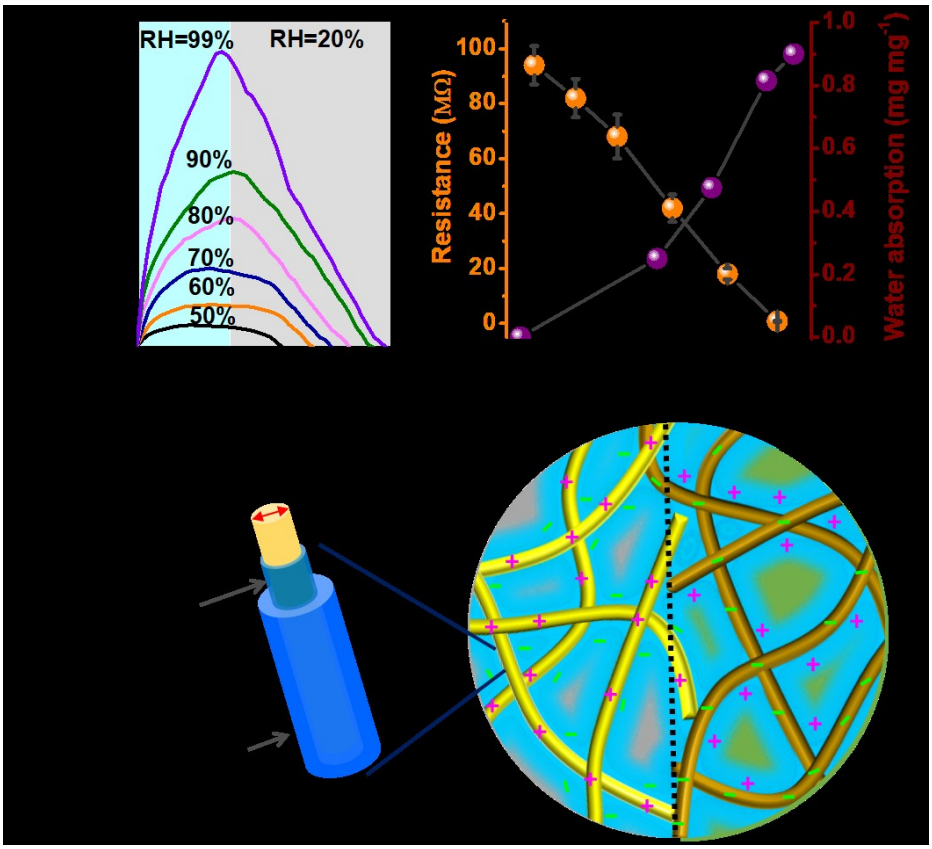

Fig. 2. Electricity-generation mechanism of asymmetric ionic aerogel. (a) V_{oc} variation upon exposing to different RHs. (b) Capacity of water absorption and internal resistance at different RHs. Carboxyl content of TEMPO-CNFs: ~0.89 mmol g^{-1}; Quaternary ammonium group of Quatern-CNFs: ~0.91 mmol g^{-1}. Generator diameter: 2 cm; Thickness: 6 mm; Bilayer thickness ratio: ~1; RH=99%. (c) Schematic illustration of voltage induced by directional movement and neutralization of free ions within hydrated charged nanochannels.

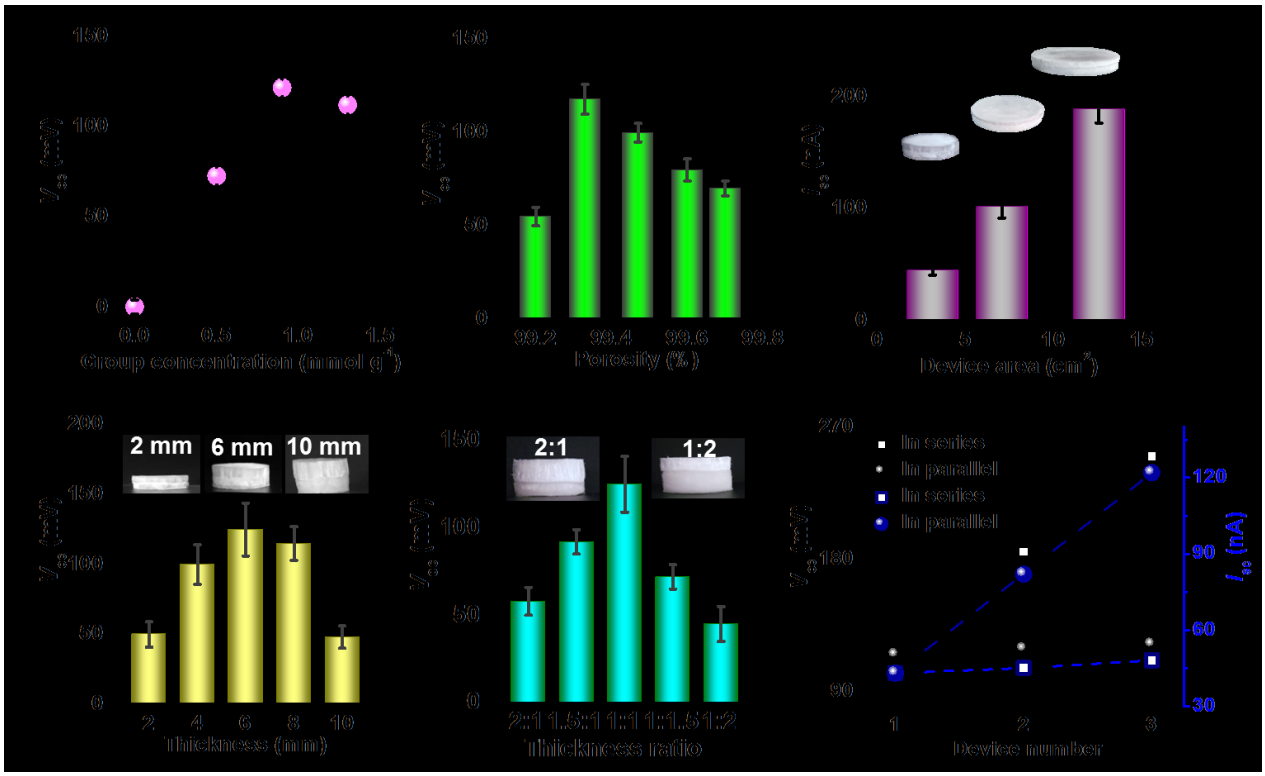

Fig. 3. Structural optimization of asymmetric ionic aerogel nanogenerator. (a) Effect of charged group content on equilibrium V_{oc}. (b) Effect of aerogel porosity on V_{oc}. (c) Effect of aerogel area on V_{oc}. (d) Effect of aerogel thickness on V_{oc}. (e) Effect of thickness ratio of TEMPO-CNFs/Quatern-CNFs layers on V_{oc}. (f) V_{oc} and I_{sc} of generators in series and parallel. Generator diameter: 2 cm; Thickness: 6 mm; Thickness ratio: ~1; RH =99%.

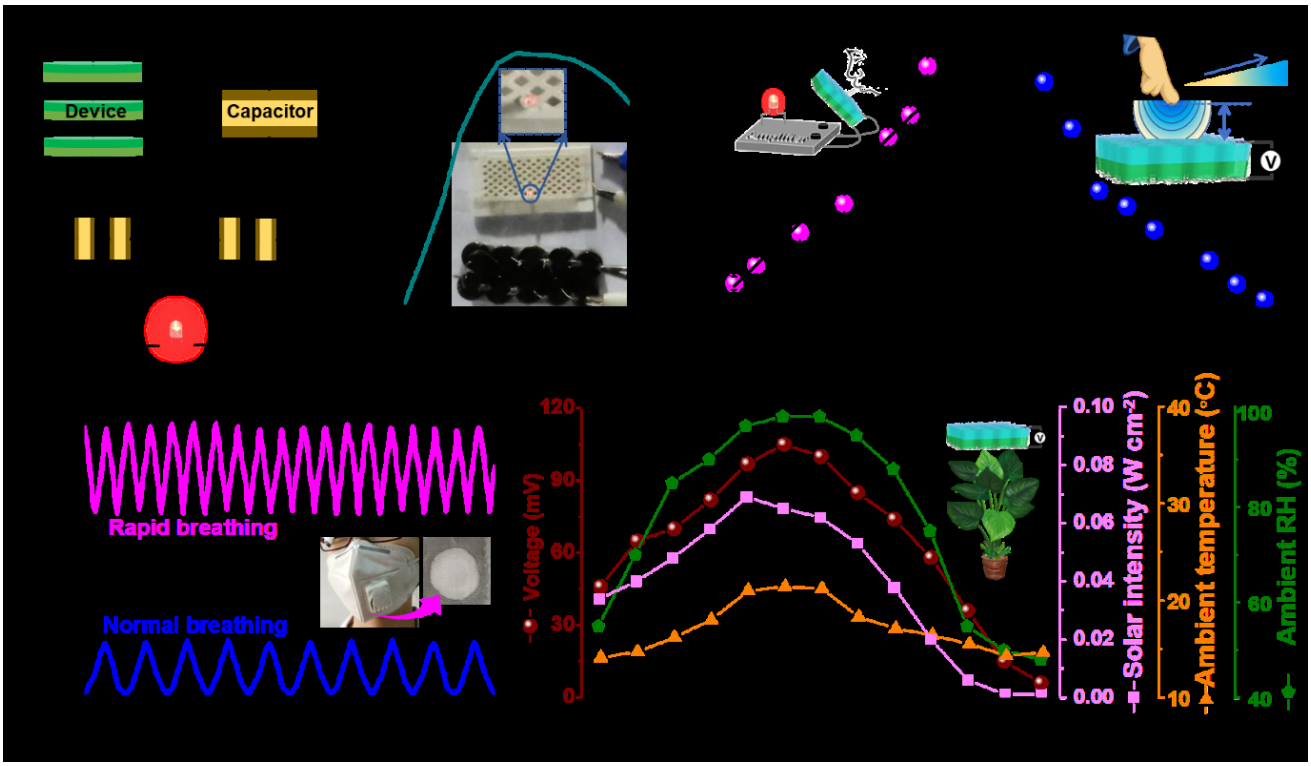

Fig. 4. Electricity-generation performance of asymmetric ionic aerogel nanogenerator. (a) Charging commercial capacitors with biological generator in series and parallel (Left) and discharging curve (Right). The inset shows a commercial red LED was powered by capacitors. (b) Asymmetric ionic aerogel nanogenerator serving as electrical humidity sensor. (c) Asymmetric ionic aerogel nanogenerator to sense finger distance. (d) V_{oc} variation when exposing to respiration (N, Frequency) settled on commercial aspirator. (e) V_{oc} variation when exposing to transpiration hanged above an *Alocasia macrorrhiza* at natural conditions (Beijing Time 8-20 o'clock, Qingdao in North China, Daytime on Apr. 26th, 2019). Generator diameter: 2 cm; Thickness: 6 mm; Thickness ratio: ~1.